C: Surfaces, Interfaces, Porous Materials, and Catalysis

Electronic Structural Origin of the Catalytic Activity Trend of Transition Metals for Electrochemical Nitrogen Reduction

Byung Chul Yeo, Jimin Kong, Donghun Kim, William A. Goddard, Hyun S. Park, and Sang Soo Han

J. Phys. Chem. C, **Just Accepted Manuscript** • Publication Date (Web): 02 Dec 2019

Electronic Structural Origin of the Catalytic Activity Trend of Transition Metals for Electrochemical Nitrogen Reduction

Byung Chul Yeo,[†,‖] Jimin Kong,[‡,‖] Donghun Kim,[†] William A. Goddard III,[§] Hyun S. Park,[‡,] and Sang Soo Han[†,*]*

[†]Computational Science Research Center, Korea Institute of Science and Technology, 5 Hwarangno 14-gil, Seoul 02792, Republic of Korea

[‡]Fuel Cell Research Center, Korea Institute of Science and Technology, 5 Hwarangno 14-gil, Seoul 02792, Republic of Korea

[§]Materials and Process Simulation Center, California Institute of Technology, Pasadena, California 91125, United States

[‖]These authors contributed equally.

*Corresponding Authors: sangsoo@kist.re.kr (SSH); hspark@kist.re.kr (HSP)

Abstract

As an alternative to the conventional Haber-Bosch process for NH_3 synthesis that operates under harsh conditions, an electrochemical process has recently been pursued. Here, using a joint experiment-density functional calculation approach, we determine the activity trend of four transition metals (TMs) (Fe, Ru, Rh, and Pd) for N_2 reduction to NH_3: Fe > Ru > Pd > Rh, where the protonation step of $*N_2$ to form $*N_2H$ (* indicates surface sites) is a potential determining step (PDS). The activity trend of the electrocatalysts is determined by the ability of the adsorbate ($*N_2$) over the catalyst surfaces to easily obtain electrons at the PDS with an assumption of a scaling relationship between the activation energy barrier and the free energy difference. In electronic structures, the ability can be estimated by the energy difference between the LUMO (lowest unoccupied molecular orbital) of the adsorbed N_2 on the TM surfaces and the fermi energy (E_F). For early TMs (e.g., Sc and Ti) where the PDS is *NH protonation reaction to form $*NH_2$, the activity of the TMs can be similarly explained with an electronic structural feature that is the energy difference between the LUMO of the *NH and the E_F. Based on the origin, we additionally consider ten TMs (Ni, Cr, Mn, Co, Cu, Mo, Ag, W, Pt, and Au) and then determine the activity trend of the total sixteen diverse TMs for NH_3 synthesis. We expect that this work could pave the way to novel alloy catalysts with a high activity for electrochemical NH_3 synthesis.

1. Introduction

As an alternative to the conventional Haber-Bosch process for ammonia (NH_3) synthesis operated at high pressure (150-300 atm) and high temperature (400-500 °C),[1,2] an electrochemical process has recently been pursued due to its low energy consumption (basically low pressure, low temperature approach) and eco-friendly environment.[3-6] The electrochemical process operates via an associative nitrogen reduction reaction (NRR) in which nitrogen molecules (N_2) are hydrogenated by protons,[7-16] as opposed to the dissociative mechanism of N_2 in the Haber-Bosch process.[17-20] Of the several elemental steps in the NRR, a few of potential determining steps (PDSs) were reported for transition metal (TM) catalysts,[21-23] in particular, the reduction of $*N_2$ to form $*N_2H$ (where * indicates a surface site) versus *NH protonation to form $*NH_2$ or $*NH_2$ protonation to form $*NH_3$, which depends on the types of the TMs when the associative mechanism has been considered on the close-packed surfaces of the TMs.[22] However, the origin of NRR activity is still unclear. An electronic structure calculation such as density-functional theory (DFT) can be significantly useful to understand the origin. In particular, since the associative NRR involves an electron transfer to adsorbed N_2 during chemical reactions, it can be expected that electrocatalyst activities can be determined by the ability of the adsorbate (e.g., $*N_2$ or *NH) over the catalyst surfaces to easily obtain electrons, which can be explained in their electronic structures.

For better understanding of the NRR mechanism and the improved design of highly active NRR catalysts, it is essential to explore and understand the activity trend of TMs as the simplest system. Although DFT studies on the activity trend have been reported,[21-23] an experimental investigation ascribed by the DFT calculations is very limited. Besides, the activity trend of Ru and Fe is widely debated,[3,22,24] and many researchers still have a question; what really is the most active TM for the NRR? Herein, we perform a joint theory-experiment study to

determine the activity trend. During the electrochemical NH_3 synthesis, the NRR competes with the hydrogen evolution reaction (HER), leading to the selectivity issue. However, in this work, we focus on the activity property of TMs. We unveil the origin of the catalytic activity of four TMs (Fe, Ru, Rh, and Pd) for NRR to NH_3. Based on the origin, we expand the theoretical approach to 12 other TMs (Sc, Ti, Ni, Cr, Mn, Co, Cu, Mo, Ag, W, Pt, and Au) and then summarize the activity trend of the 16 total TMs for NH_3 synthesis. To the best of our knowledge, this study reports the first direct comparison between experimental and theoretical activities of various TMs for the NH_3 synthesis.

2. Methods

2.1. Computational Details

To investigate the associative NRR mechanism over TM surfaces, we used DFT calculations and obtained free energy diagrams for all possible reaction intermediates. The DFT calculations were performed using the Vienna ab initio simulation package (VASP) with projector-augmented wave pseudopotentials and the RPBE (revised Perdew-Burke-Ernzerhof) functional,[25-27] where the plane-wave kinetic energy cutoff was 520 eV. During the DFT calculation, the spin-polarized condition and the van der Waals interaction (Grimme's DFT-D3 method) were adopted.[28] For the TM surfaces, we considered close-packed surfaces of each crystal structure: (111) for fcc metals (Pd, Rh, Ni, Mn, Cu, Ag, Pt, and Au), (001) for hcp (Ru, Sc, Ti, and Co), and (110) for bcc (Fe, Cr, Mo, and W). The flat surfaces were modeled with four-layer slabs repeated periodically with a 3×3 unit cell, and the 4×4×1 Monkhorst-Pack *k*-point mesh was used.[29] The top two layers of the slab models and the adsorbates were allowed to relax until the forces on the individual relaxed atoms were less than 0.05 eV $Å^{-1}$, while the

bottom two layers were fixed during the optimization process. Moreover, a free energy correction was considered using a standard vibrational correction in the harmonic approximation to enthalpy and entropy. Additionally, solvation effects were not included because the solvation-induced stabilization of adsorbates in the NRR is within 0.1 eV of the theoretical overpotentials for each TM.[22] Details can be found in the Supporting Information (SI).

2.2. Experimental Section

We also electrochemically measured NH_3 production rates to estimate catalytic activities of Fe, Ru, Pd, and Rh nanoparticles (NPs), in which the TM catalysts were purchased as metallic catalysts and used after a reductive thermal treatment and all of them have spherical shapes (Fig. S5). Details on the TM catalysts and the reductive thermal treatments are additionally explained in the SI. Colorimetrtic analysis of the produced NH_3 allows quantification of the electrochemical NRR activity on different TM surfaces (Figs. S7-S10). According to the Wulff construction based on surface energies of the TM metals,[30,31] the exposed surfaces in the spherical NPs are mostly close-packed surfaces. This justifies the use of the close-packed surfaces in the present DFT calculations. No oxide layer on the TM surfaces can be presumed under the operating conditions of our electrochemical measurements, i.e., negative applied potentials under reducing environments (Fig. S11). The electrochemical NH_3 synthesis was carried out in a single-cell environment. An anion exchange membrane was used as the solid electrolyte separator in an electrolytic cell. Fe, Ru, Rh, and Pd were investigated as the cathode catalyst, and IrO_2 was fixed as an anode catalyst. The MEA (membrane electrode assembly) was constructed with an anion exchange membrane electrolyte embedded between the cathode and the anode. The NRR was performed at the cathode under gaseous humidified N_2 atmosphere at

338 K, while 0.5M KOH solution was supplied to the anode for water oxidation. The NH_3 produced at the cathode was transported to the external acid trap of 10 mM H_2SO_4 aqueous solution. The acid trap solution prevented the leakage of NH_3 gas into the air, and the concentration of NH_4^+ in the trap was evaluated. Experimental details can be also found in the SI. In addition, nuclear magnetic resonance (NMR) measurements were conducted to clarify the source of NH_3 existed in the trap solution. ^1H NMR spectra were obtained for the post-electrolysis 0.1 M KOH electrolyte using Pd/C coated carbon paper with ^{14}N as the feeding gas and deuterium oxide (D_2O, Sigma Aldrich) was used as lock agent. Before the NMR measurement, pH of electrolyte (0.1 M KOH) was adjusted using 1 M H_2SO_4. In the NMR Spectra, a triplet coupling for $^{14}NH_4^+$ was observed for the $^{14}N_2$ saturated electrolyte.

3. Results and discussion

3.1. The activity trend of Fe, Ru, Pd, and Rh

Free-energy diagrams for the associative NRR mechanism on Fe(110), Ru(001), Pd(111), and Rh(111) are shown in Fig. 1. From the 2nd protonation, two reaction pathways are possible; i.e., $*N_2H_2$ can be either $*NNH_2$ or *NHNH. Our DFT calculation reveals that the $*NNH_2$ formation is more thermodynamically plausible over the TM surfaces than the *NHNH formation. It is worth noting that among several elementary steps, the change of free energies ($\triangle G_{*N2H}$-$\triangle G_{*N2}$) between $*N_2$ and $*N_2H$ molecules on the TM surfaces is the highest. This implies that this step would be the PDS for NH_3 synthesis. Since $\triangle G_{*N2H}$-$\triangle G_{*N2}$ is 0.80 eV for Fe(110), 1.41 eV for Ru(001), 1.57 eV for Pd(111), and 1.71 eV for Rh(111), it is expected that their activity trend for NH_3 synthesis would be Fe(110) > Ru(001) > Pd(111) > Rh(111), based on the Brønsted-Evans-Polanyi relation indicating a linear relation between the activation energy

and the reaction energy.[32,33] For comparison, we also investigated free energy diagrams for N_2 reduction over Fe(111), Fe(100), Ru(111), and Ru(110) surfaces (Figs. S3 and S4) and then found that for the Fe and Ru surfaces, the $*N_2H$ formation reaction is the PDS, as observed on Fe(110) and Ru(001). Based on $\triangle G_{*N2H}$-$\triangle G_{*N2}$, it can be expected that the activity trend is Fe(111) (0.47 eV) > Fe(110) (0.80 eV) > Fe(100) (0.98 eV) > Ru(111) (1.10 eV) > Ru(001) (1.41 eV) > Ru(110) (2.12 eV), in which the Fe surfaces show a higher activity than Ru surfaces because all of the energy differences on the three Fe surface are lower than those on Ru surfaces.

To test the theoretical activity trend in experiments, the NH_3 production rates over Fe, Ru, Pd, and Rh NP surfaces were examined in the two-electrode device. Since the Fe, Ru, Pd, and Rh NP sizes are not identical (Fig. S5), we used Brunauer-Emmett-Teller (BET) surface area normalized NH_3 production rates for assessing the intrinsic activity of the catalyst. Instead of the BET surface area, electrochemical active surface area can be also considered to obtain the catalytic activity. However, it is very challenging to determine the actual surface areas of active catalysts without the contribution of inactive carbon supports during electrochemical measurements. When the TM catalysts are supported on the porous carbon paper for electrochemical tests, the obtaining charging current includes both of the contributions from activated carbon used as a support and from the carbon paper used as the electrode substrate. Accordingly, in this work, we used the BET normalized activity.

The mass activities, the faraday efficiency (FE) values, and the BET area-normalized NH_3 production rates (r_{NH3}) are summarized in Table 1. The NRR activity trend displayed in the experiment is indeed Fe > Ru > Pd > Rh, as theoretically predicted with the limiting potential (U_L) that is determined as the negative of ΔG^*_{N2H}-ΔG^*_{N2} when the PDS is $*N_2 \rightarrow *N_2H$ (Fig. 2). In this study, gaseous N_2 was supplied to the TM cathodes to reveal the NRR kinetic without

mass transport limitation of N_2. However, the faraday efficiencies toward NH_3 production were still limited to approximately 4.15, 0.23, 0.25, and 0.21% for Fe, Ru, Pd, and Rh NPs, respectively, and the HER occurs dominantly. The proton reduction kinetics can be faster than those of NRR, with a smaller number of electrons and atoms involved in the electrode reaction, if no HER inhibitor or aprotic solvent is employed.[34,35] In this study, reduction of the HER activity using the aprotic or cationic inhibitors was not particularly pursued, but only the specific adsorption of N_2 to TMs is considered. We also note that no hydrazine as a possible by-product of NRR was observed during the measurements in the colorimetric analysis. Furthermore, according to our NMR experiments, no triplet peaks corresponding to $^{14}NH_4^+$ were observed from the NMR spectra under Ar feeding conditions, although the peaks were observed with $^{14}N_2$ as the feeding gas (Fig. S12). A possibility for NH_4^+ production from the reduction of NO_x ions in the electrolyte, which has been recently issued,[36,37] can be regarded to be insignificant because no $^{14}NH_4^+$ were detected under Ar atmosphere in the NMR measurements. As a result, this implies no significant interference in the colorimetric determination of NH_4^+ and supports that the NH_3 is indeed produced from the feeding N_2 gases.

According to the reported volcano plot between the theoretical limiting potential for N_2 electroreduction of Fe, Ru, Pd and Rh,[21] the activity for NH_3 synthesis shows the following trend: Fe(110) > Ru(001) > Rh(111) > Pd(111). However, both of our experiments and DFT calculations with the investigation of diverse adsorption sites of N_2 and N_2H for Fe, Ru, Rh, and Pd show that the Rh catalyst shows the lower activity than Fe, Ru, and Pd (Fig. 2). In this regard, we clarified that the activity trend of Fe, Ru, Pd and Rh catalysts is correlated with the $\triangle G_{*N2H}$-$\triangle G_{*N2}$ value.

To understand the origin of the activity trend of the Fe, Ru, Pd, and Rh TMs, we focused on the electronic structures of N_2 adsorbed on the TM surfaces (Fig. 3). Because the PDS for electrochemical NH_3 synthesis over the TM surfaces is a protonation reaction of $*N_2$ ($*N_2 + H^+ + e^- \rightarrow *N_2H$), their catalytic activities are determined by the ability of N_2 adsorbed on the catalyst surfaces to easily obtain electrons. In electronic structures, the ability can be estimated by the energy difference between the LUMO (lowest unoccupied molecular orbital) of the adsorbed N_2 on the TM surfaces and the fermi energy (E_F). In the gas phase, the LUMO of N_2 is π_{2p}^*. Upon adsorption of N_2 over the TM surfaces, the π_{2p}^* orbital of N_2 is hybridized with *d* orbitals of the TMs, leading to a shift to lower energy levels. The energy difference between the LUMO and the E_F follows a trend of Fe(110) < Ru(001) < Pd(111) < Rh(111); i.e., electrons can most easily occupy the LUMO over Fe(110) during the protonation of N_2 and with the opposite true over Rh(111), which indeed follows the experimental activity trend in Fig. 2.

3.2. The activity trend of early TMs (e.g., Sc and Ti)

To expand the correlation between the activity of TMs and the electronic structural feature, we additionally considered early TMs, such as Sc and Ti, because these TMs are reported to have a different PDS from those of Fe, Ru, Pd, and Rh, i.e., *NH protonation to form $*NH_2$ ($*NH + H^+ + e^- \rightarrow *NH_2$).[10] This was also confirmed by our DFT calculations on the electrochemical NRR mechanisms over Sc(001) and Ti(001) (Fig. 4). For these cases, the catalytic activity can be estimated by the energy difference between the LUMO of the *NH on the TM surfaces and E_F, where the LUMO of the NH radical in the gas phase has the *p* orbital character in the N atom and it is hybridized with *d* orbitals of the TMs upon adsorption. The energy difference is 1.31 eV over Sc(001) and 1.02 eV over Ti(001) in Fig. 3, implying a higher NRR activity over Ti(001) than over Sc(001). Indeed, in their energy profiles for the NRR (Fig.

4), the energy difference for $*NH + H^+ + e^- \rightarrow *NH_2$ is smaller over Ti(001). Additionally, by comparing the LUMO energies of $*N_2$ and *NH over Sc(001) and Ti(001) (e.g., for Sc(001), 0.20 eV for $*N_2$ versus 1.31 eV for *NH), it is clear that over the TM surfaces, an electron addition into *NH is harder than that into $*N_2$, which indicates that the PDS over the TM surface is observed to be the step for the protonation of *NH rather than the protonation of $*N_2$. Conversely, over Fe(110), Ru(001), Pd(111), and Rh(111) surfaces, an electron addition into $*N_2$ is harder than that into *NH.

3.3. Determination of sixteen diverse TMs

From the results discussed so far, the catalytic activity on flat surfaces of TMs can be estimated by comparing the following two free energy differences: $\triangle G_{*N2H}$-$\triangle G_{*N2}$ versus $\triangle G_{*NH2}$-$\triangle G_{*NH}$. Of course, as already mentioned, stepped surfaces can show a different PDS, such as $*NH_2$ protonation to form $*NH_3$.[22] The exposed surfaces in the spherical NPs are mostly close-packed surfaces according to the Wulff construction based of surface energies of the TM metals.[30,31] Thus, we focus on the flat surfaces of TMs in this work. By additionally calculating the free energy change, we determined the activity trend for NH_3 synthesis of sixteen TMs (Fig. 5). For a given TM surface, as both of the free energy changes approach zero, the TM shows a high catalytic activity. From Fig. 5, we determined the activity trend of the sixteen TMs to be Fe(111) > W(110) > Fe(110) > Mo(110) > Fe(100) > Cr(110) > Mn(110) > Ru(001) > Ti(001) > Pt(111) > Sc(001) > Co(001) > Pd(111) > Ni(111) > Rh(111) > Cu(111) > Au(111) > Ag(111). In addition, we need to compare the activity trend of Fe and Ru, as their activity trend for electrochemical NH_3 synthesis has been still controversial.[3,22,24] According to our joint experiment-theory study, Fe shows a higher activity than Ru, at least for low index surfaces, in

which all of Fe(110), Fe(100), and Fe(111) surfaces have a higher activity performance than Ru(001), Ru(110), and Ru(111).

4. Conclusion

In conclusion, we have studied the activity trend of Fe, Ru, Rh, and Pd TM catalysts for the electrochemical NRR both experimentally and theoretically, where the trend follows Fe > Ru > Pd > Rh . The activity trend can be explained by the energy difference between the LUMO of the adsorbed N_2 and E_F, based on the fact that the PDS over the TMs is the protonation step of N_2 adsorbed over the surfaces. On the other hand, the PDS over early TMs, such as Sc or Ti, is found to be the protonation step of *NH. Thus, their activity can be estimated by the energy difference between the LUMO of the *NH and E_F. Based on the above results, we have also determined an activity trend of 16 TM surfaces. We expect that this work could pave the way to novel catalysts with a high activity for electrochemical NH_3 synthesis.

Acknowledgment

This work was supported by Creative Materials Discovery Program through the National Research Foundation of Korea (NRF-2016M3D1A1021141).

ASSOCIATED CONTENT

Supporting Information Available: Details and additional results on DFT calculations and the electrochemical experiments.

AUTHOR INFORMATION

Corresponding Authors

*E-mail: sangsoo@kist.re.kr (SSH)

*E-mail: hspark@kist.re.kr (HSP)

Author Contributions

‖These authors contributed equally.

Notes

The authors declare no competing financial interest

References

(1) Smil, V. Enriching the Earth: Fritz Haber, Carl Bosch, and the Transformation of World Food Production; MIT Press: Cambridge, MA **2004**.

(2) Jennings, J. R. Ed. Catalytic Ammonia Synthesis: Fundamentals and Practice, Springer Science & Business Media: New York **2013**.

(3) Renner, J. N.; Greenlee, L. F.; Ayres, K. E.; Herring, A. M. Electrochemical Synthesis of Ammonia: A Low Pressure, Low Temperature Approach. *Electrochem. Soc. Interface* **2015**, *24*, 51−57.

(4) Shipman, M. A.; Symes, M. D. Recent Progress Towards the Electrosynthesis of Ammonia from Sustainable Resources. *Catal. Today* **2017**, *286*, 57−68.

(5) Kyriakou, V.; Garagounis, I.; Vasileiou, E.; Vourros, A.; Stoukides, M. Progress in the Electrochemical Synthesis of Ammonia. *Catal. Today* **2017**, *286*, 2−13.

(6) Guo, C.; Ran, J.; Vasileff, A.; Qiao, S. Z. Rational Design of Electrocatalysts and Photo(electro)catalysts for Nitrogen Reduction to Ammonia (NH_3) Under Ambient Conditions. *Energy Environ. Sci.* **2018**, *11*, 45−56.

(7) Nash, J.; Yang, X.; Anibal, J.; Wang, J.; Yan, Y.; Xu, B. Electrochemical Nitrogen Reduction Reaction on Noble Metal Catalysts in Proton and Hydroxide Exchange Membrane Electrolyzers. *J. Electrochem. Soc.* **2017**, *164*, F1712−F1716.

(8) Wang, J.; Yu, L.; Hu, L.; Chen, G.; Xin, H.; Feng, X. Ambient Ammonia Synthesis Via Palladium-Catalyzed Electrohydrogenation of Dinitrogen at Low Overpotential. *Nat. Commun*. **2018**, *9*, 1795(1)-(7).

(9) Shi, M.-M.; Bao, D.; Wulan, B.-R.; Li, Y.-H.; Zhang, Y.-F.; Yan, J.-M.; Jiang, Q. Au Sub-Nanoclusters on TiO_2 toward Highly Efficient and Selective Electrocatalyst for N_2 Conversion to NH_3 at Ambient Conditions. *Adv. Mater.* **2017**, *29*, 1606550(1)-(6).

(10) Bao, D.; Zhang, Q.; Meng, F.-L.; Zhong, H.-X.; Shi, M.-M.; Zhang, Y.; Yan, J.-M.; Jiang, Q.; Zhang, X.-B. Electrochemical Reduction of N_2 under Ambient Conditions for Artificial N_2 Fixation and Renewable Energy Storage Using N_2/NH_3 Cycle. *Adv. Mater.* **2017**, *29*, 1604799(1)-(5).

(11) Chen, S.; Perathoner, S.; Ampelli, C.; Mebrahtu, C.; Su, D.; Centi, G. Electrocatalytic Synthesis of Ammonia at Room Temperature and Atmospheric Pressure from Water and Nitrogen on a Carbon-Nanotube-Based Electrocatalyst. *Angew. Chem. Int. Ed.* **2017**, *129*, 2743−2747.

(12) Kong, J.; Lim, A.; Yoon, C.; Jang, J. H.; Ham, H. C.; Han, J.; Nam, S.; Kim, D.; Sung, Y.-E.; Choi, J.; Park, H. S. Electrochemical Synthesis of NH_3 at Low Temperature and Atmospheric Pressure Using a γ-Fe_2O_3 Catalyst. *ACS Sustainable Chem. Eng.* **2017**, *5*, 10986−10995.

(13) Li, S.-J.; Bao, D.; Shi, M.-M.; Wulan, B.-R.; Yan, J.-M.; Jiang, Q. Amorphizing of Au Nanoparticles by CeO_x−RGO Hybrid Support towards Highly Efficient Electrocatalyst for N_2 Reduction under Ambient Conditions. *Adv. Mater.* **2017**, *29*, 1700001(1)-(6).

(14) Kim, K.; Yoo, C.-Y.; Kim, J.-N.; Yoon, H. C.; Han, J.-I. Electrochemical Synthesis of Ammonia from Water and Nitrogen in Ethylenediamine Under Ambient Temperature and

Pressure. *J. Electrochem. Soc.* **2016**, *163*, F1523-F1526.
(15) Lan, R.; Irvine, J. T. S.; Tao, S. Synthesis of Ammonia Directly from Air and Water at Ambient Temperature and Pressure. *Sci. Rep.* **2013**, *3*, 1145(1)-(7).
(16) Greenlee, L. F.; Renner, J. N.; Foster, S. L. The Use of Controls for Consistent and Accurate Measurements of Electrocatalytic Ammonia Synthesis from Dinitrogen. *ACS Catal.* **2018**, *8*, 7820−7827
(17) Mortensen, J. J.; Hammer, B.; Nørskov, J. K. Alkali Promotion of N_2 Dissociation over Ru(0001). *Phys. Rev. Lett.* **1998**, *80*, 4333-4336.
(18) Honkala, K.; Hellman, A.; Remediakis, I. N.; Logadottir, A.; Carlsson, A.; Dahl, S.; Christensen, C. H.; Nørskov, J. K. Ammonia Synthesis from First-Principles Calculations. *Science* **2005**, *307*, 555-558.
(19) Mehta, P.; Barboun, P.; Herrera, F. A.; Kim, J.; Rumbach, P.; Go, D. B.; Hicks, J. C.; Schneider, W. F. Overcoming Ammonia Synthesis Scaling Relations with Plasma-Enabled Catalysis. *Nat. Catal.* **2018**, *1*, 269-275.
(20) Qian, J.; An, Q.; Fortunelli, A.; Nielsen, R. J.; Goddard, W. A. III, Reaction Mechanism and Kinetics for Ammonia Synthesis on the Fe(111) Surface. *J. Am. Chem. Soc.* **2018**, *140*, 6288-6297.
(21) Skúlason, E.; Bligaard, T.; Gudmundsdóttir, S.; Studt, F.; Rossmeisl, J.; Abild-Pedersen, F.; Vegge, T.; Jónsson, H.; Nørskov, J. K. A Theoretical Evaluation of Possible Transition Metal Electro-Catalysts for N_2 Reduction. *Phys. Chem. Chem. Phys.* **2012**, *14*, 1235-1245.
(22) Montoya, J. H.; Tsai, C.; Vojvodic, A.; Nørskov, J. K. The Challenge of Electrochemical Ammonia Synthesis: A New Perspective on the Role of Nitrogen Scaling Relations. *ChemSusChem.* **2015**, *8*, 2180-2186.
(23) Back, S.; Jung, Y. On the Mechanism of Electrochemical Ammonia Synthesis on the Ru Catalyst. *Phys. Chem. Chem. Phys.* **2016**, *18*, 9161-9166.
(24) van der Ham, C. J. M.; Koper, M. T. M.; Hetterscheid, D. G. H. Challenges in Reduction of Dinitrogen by Proton and Electron Transfer. *Chem. Soc. Rev.* **2014**, *43*, 5183-5191.
(25) Kresse, G.; Joubert, D. From Ultrasoft Pseudopotentials to the Projector Augmented-Wave Method. *Phys. Rev. B.* **1999**, *59*, 1758-1775.
(26) Hammer, B.; Hansen, L. B.; Nørskov, J. K. Improved Adsorption Energetics within Density-Functional Theory Using Revised Perdew-Burke-Ernzerhof Functionals. *Phys. Rev. B.* **1999**, *59*, 7413-7421.
(27) Blochl, P. E. Projector Augmented-Wave Method. *Phys. Rev. B.* **1994**, *50*, 17953-17979.
(28) Moellmann, J.; Grimme, S. DFT-D3 Study of Some Molecular Crystals. *J. Phys. Chem. C.* **2014**, *118*, 7615-7621.
(29) Monkhorst, H. J.; Pack, J. D. Special Points for Brillouin-Zone Integrations. *Phys. Rev. B.* **1976**, *13*, 5188-5192.
(30) Tran, R.; Xu, Z.; Radhakrishnan, B.; Winston, D.; Sun, W.; Persson, K. A.; Ong, S. P. Data Descriptor: Surface Energies of Elemental Crystals. *Sci. Data* **2016**, *3*, 160080(1)-(13).
(31) Liu, X.; Wen, X.; Hoffmann, R. Surface Activation of Transition Metal Nanoparticles for Heterogeneous Catalysis: What We Can Learn from Molecular Dynamics. *ACS Catal.* **2018**, *8*, 3365-3375.
(32) Abild-Pedersen, F.; Greeley, J.; Studt, F.; Rossmeisl, J.; Munter, T. R.; Moses, P. G.; Skúlason, E.; Bligaard, T.; Nørskov, J. K. Scaling Properties of Adsorption Energies for

Hydrogen-Containing Molecules on Transition-Metal Surfaces. *Phys. Rev. Lett.* **2007**, *99*, 016105(1)-(4).
(33) Nørskov, J. K.; Bligaard, T.; Hvolbæk, B.; Abild-Pedersen, F. The Nature of the Active Site in Heterogeneous Metal Catalysis. *Chem. Soc. Rev.* **2008**, *37*, 2163-2171.
(34) Suryanto, B. H. R.; Kang, C. S. M.; Wang, D.; Xiao, C.; Zhou, F.; Azofra, L. M.; Cavallo, L.; Zhang, X.; MacFarlane, D. R. Rational Electrode-Electrolyte Design for Efficient Ammonia Electrosynthesis under Ambient Conditions. *ACS Energy Lett.* **2018**, *3*, 1219-1224.
(35) McEnaney, J. M.; Singh, A. R.; Schwalbe, J. A.; Kibsgaard, J.; Lin, J. C.; Cargnello, M.; Jaramillo, T. F.; Nørskov, J. K. Ammonia Synthesis from N_2 and H_2O Using a Lithium Cycling Electrification Strategy at Atmospheric Pressure. *Energy Environ. Sci.* **2017**, *10*, 1621-1630.
(36) Suryanto, B. H.R.; Du, H.-L.; Wang, D.; Chen, J.; Simonov, A. N.; MacFarlane, D. R. Challenges and Prospects in the Catalysis of Electroreduction of Nitrogen to Ammonia. *Nat. Catal.* **2019**, *2*, 290-296.
(37) Andersen, S. Z.; Čolić, V.; Yang, S.; Schwalbe, J. A.; Nielander, A. C.; McEnaney, J. M.; Enemark-Rasmussen, K.; Baker, J. G.; Singh, A. R.; Rohr, B. A.; et al. A Rigorous Electrochemical Ammonia Synthesis Protocol with Quantitative Isotope Measurements. *Nature* **2019**, *570*, 504-508.

Table 1. Mass activities, faraday efficiency (F.E.) values, and BET surface area-normalized NH_3 production rates (r_{NH3}) at the Fe, Ru, Pd, and Rh nanoparticles (NPs) for electrochemical NH_3 synthesis experiments.

Catalyst	Mass activity (mol s^{-1} mg^{-1})	F.E. (%)	BET surface area (m^2 g^{-1})	r_{NH3} (mol s^{-1} cm^{-2}_{act})
Fe NPs	2.36×10^{-11}	4.15	10.3	2.35×10^{-13}
Ru NPs	1.72×10^{-11}	0.23	61.3	0.35×10^{-13}
Pd NPs	2.53×10^{-11}	0.25	657.4	0.04×10^{-13}
Rh NPs	0.17×10^{-11}	0.21	43.7	0.02×10^{-13}

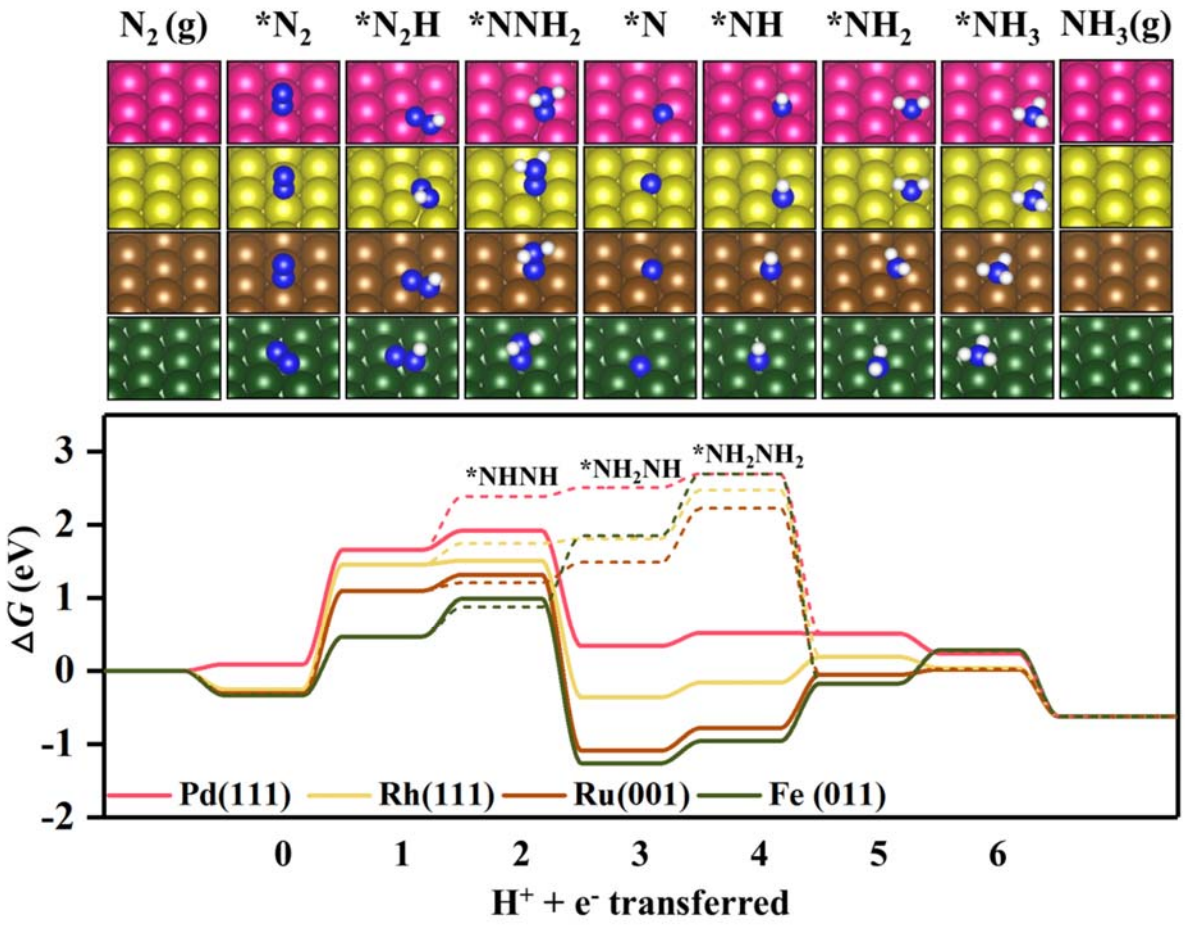

Figure 1. Free energy diagram (below) at U=0 V (vs. RHE) for the reaction intermediates that are the lowest energy structures (above) in the associative nitrogen reduction process of N_2 to NH_3. The free energy pathway consists of 7 consecutive steps for proton-coupled electron transfers from $*N_2$ to $*NH_3$. Here, from the 2nd protonation, two reaction pathways are possible; i.e., $*N_2H_2$ can be either $*NNH_2$ (solid line) or *NHNH (dotted line). The target catalytic surfaces are Fe(110), Ru(001), Rh(111), and Pd(111). Pink, yellow, brown, green, blue and white atoms indicate Pd, Rh, Ru, Fe, N and H, respectively.

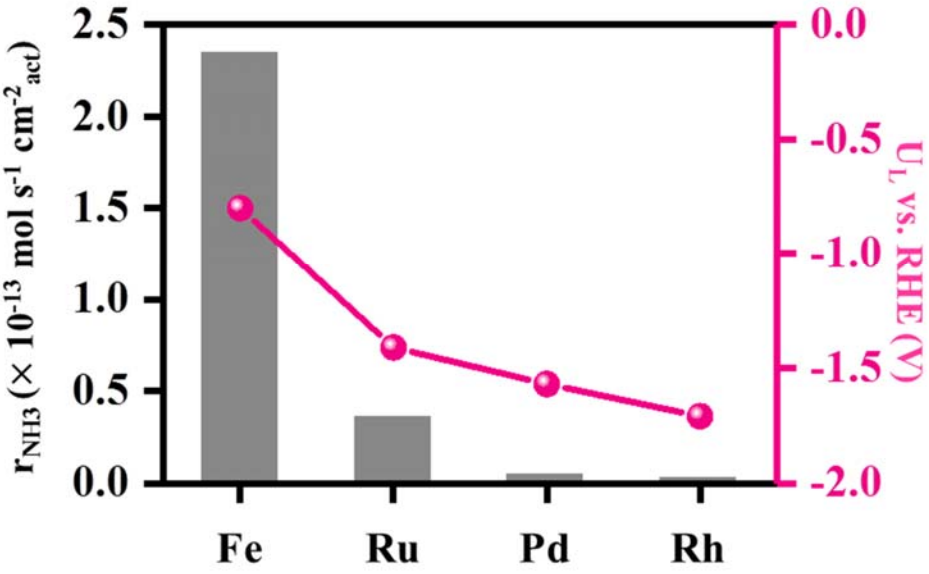

Figure 2. Comparison between the experimental BET surface area-normalized NH_3 production rates (r_{NH3}) (gray bar) and the limiting potential (U_L) (pink line) during the protonation of $*N_2$ ($*N_2 \rightarrow *N_2H$) for the Fe, Ru, Pd, and Rh metals. Here, the r_{NH3} was measured at an applied voltage of 1.3 V.

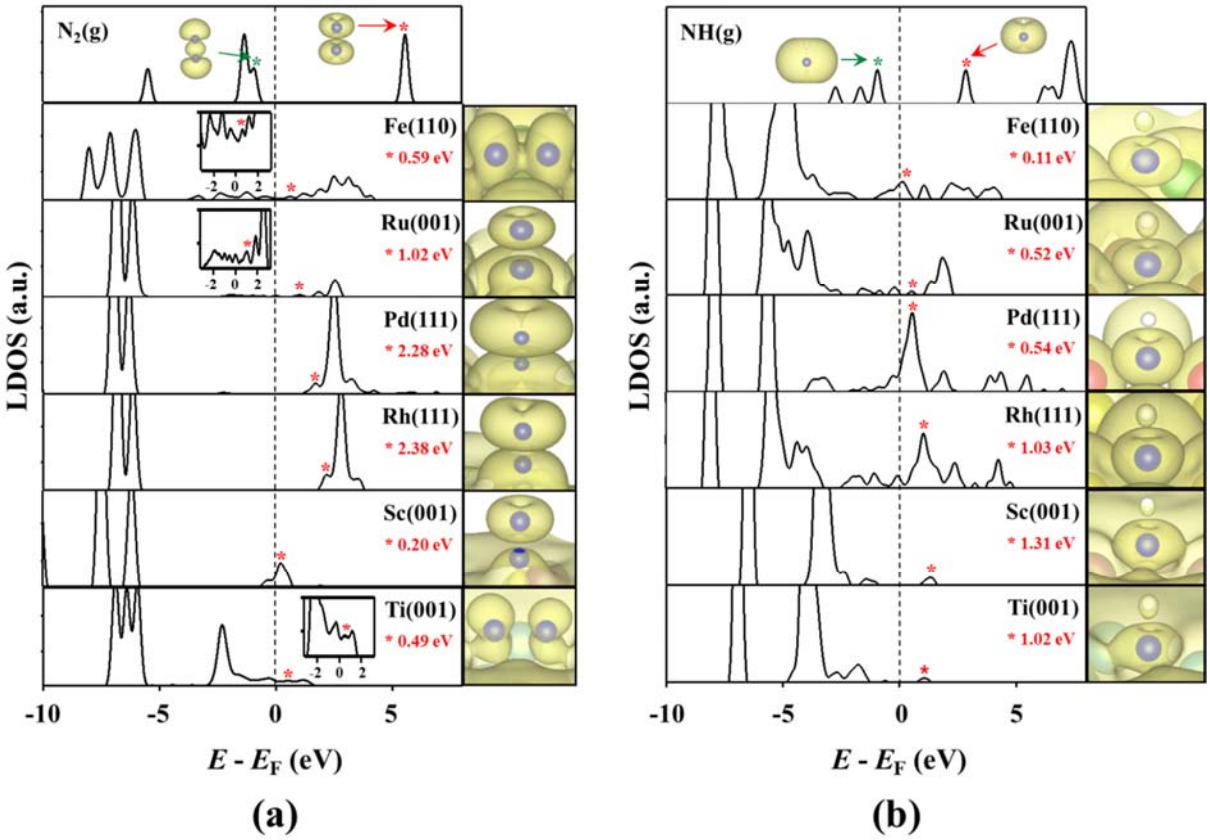

Figure 3. LDOS of (a) *N_2 and (b) *NH adsorbed on TM surfaces. In each figure, the top to bottom are for the gas phase, Fe(110), Ru(001), Pd(111), Rh(111), Sc(001), and Ti(001), respectively. The dashed line indicates the fermi level (E_F). The red value in each figure indicates the energy level (red star) of the LUMO and the green star in the figure of the gas phase indicates the energy level of the HOMO. The charge density at the energy level is shown on the right of each figure.

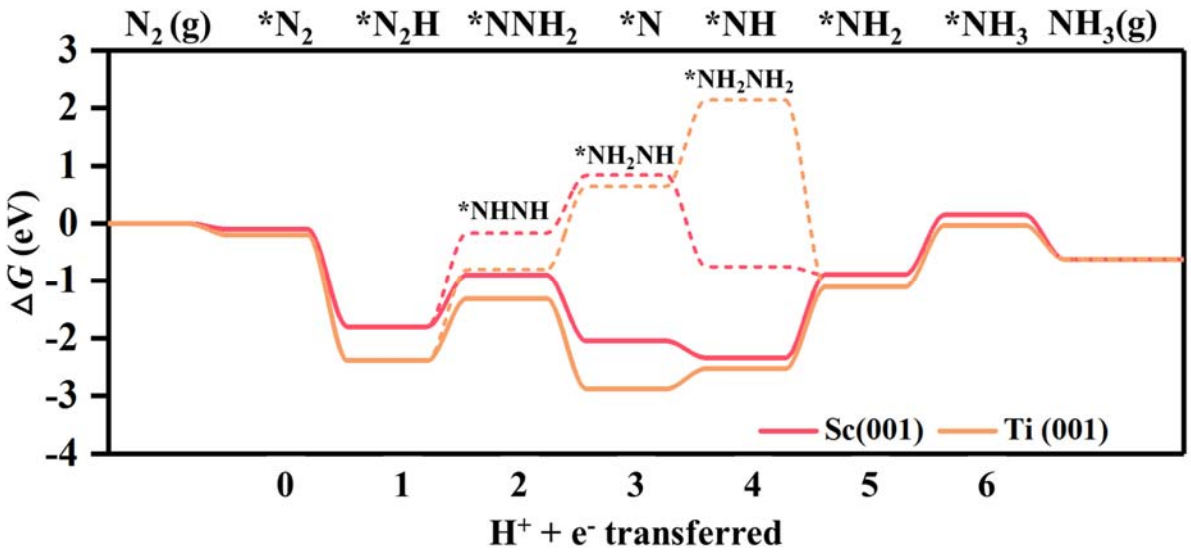

Figure 4. Free energy diagram at U=0 V (vs. RHE) for the reaction intermediate in the associative NRR process of N_2 to NH_3 on the Sc(001) (red) and Ti(001) (orange). The free energy pathway consists of 7 consecutive steps for proton-coupled electron transfers from $*N_2$ to $*NH_3$. Here, from the 2nd protonation, two reaction pathways are possible; i.e., $*N_2H_2$ can be either $*NNH_2$ (solid line) or *NHNH (dotted line).

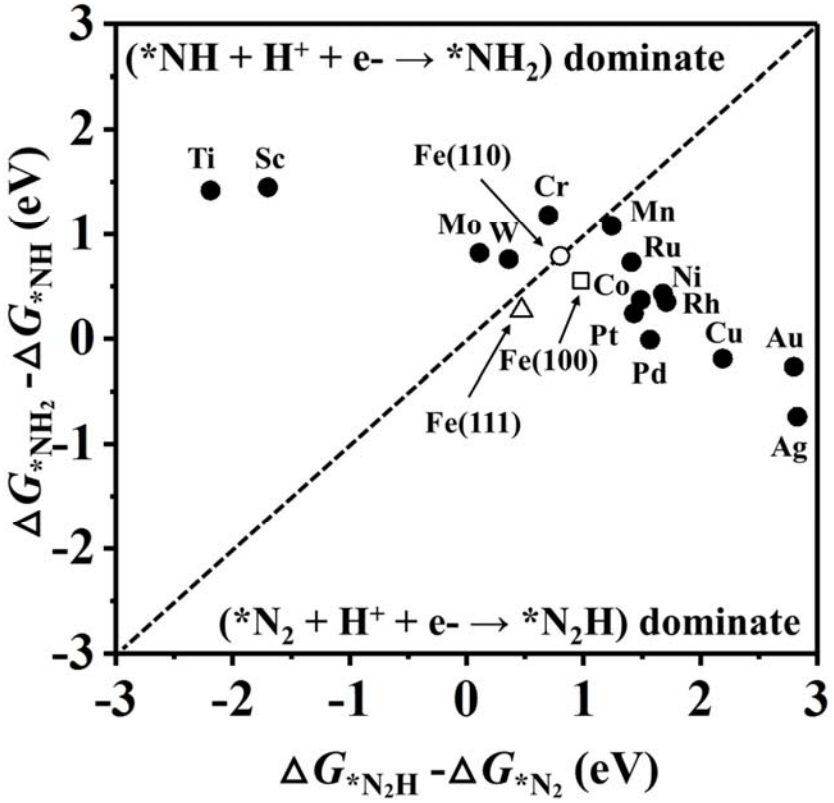

Figure 5. Comparisons with free energies between $\triangle G_{*N2H}$-$\triangle G_{*N2}$ and $\triangle G_{*NH2}$-$\triangle G_{*NH}$ for the protonation of $*N_2$ ($*N_2 \rightarrow *N_2H$) and *NH ($*NH \rightarrow *NH_2$) over various TM surfaces during the associative NRR processes. The dashed lines indicate equally dominant protonations of $*N_2$ and *NH.

TOC Graphic

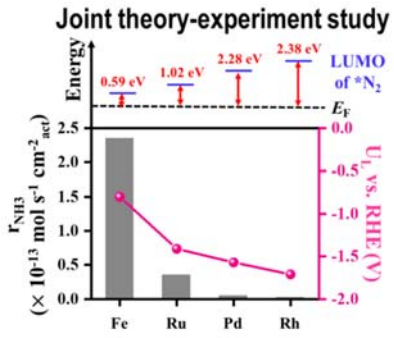
Joint theory-experiment study
Energy
0.59 eV
1.02 eV
2.28 eV
2.38 eV
LUMO of *N2
EF
2.5
2.0
1.5
1.0
0.5
0.0
0.0
-0.5
-1.0
-1.5
-2.0
U vs. RHE (V)
Fe
Ru
Pd
Rh